UC-25
LBL-6036
c. 1

MECHANICAL PROPERTIES OF DIRECTIONALLY SOLIDIFIED Al-Si EUTECTIC

Danny Gene Morrow
M. S. thesis

May 1977

Prepared for the U. S. Energy Research and Development Administration under Contract W-7405-ENG-48

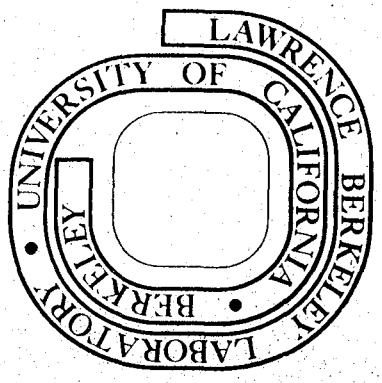

LBL-6036
c. 1

MECHANICAL PROPERTIES OF DIRECTIONALLY SOLIDIFIED Al-Si EUTECTIC

BY

Danny Gene Morrow

Lawrence Berkeley Laboratory
University of California
Berkeley, California 94720

This work was done with support from the U.S. Energy Research and Development Administration.

ABSTRACT

The effect of directional solidification on the yield strength of the Al-Si eutectic alloy has been studied. Eutectic alloys (Al-12.7 wt. % Si) were directionally frozen at growth rates, R, between 0.097 cm/h and 47.0 cm/h through a temperature gradient of about 80°C/cm. As found by Day and Hellawell (1), an oriented [001] Si fiber texture is obtained for rates less than 1.0 cm/hr, and at higher growth rates microstructures similar to the as-cast eutectic are found. At the lower growth rates, banded structures alternating rich in Si and lean in Si were also observed. Tensile measurements indicated that the yield strength is independent of R at growth rates less than ca. 1.0 cm/h, while at higher growth rates the strength increases linearly with $R^{1/4}$. Composite strengthening due to aligned Si microstructure at low R was not exhibited due to the preferential yielding within the banded structures. Yield strengths for higher growth rates are controlled by a precipitate spacing effect.

---

1. Day, M. G. and Hellawell, A. H., Proc. Royal Soc. A305, 473-491, (1971).

I. INTRODUCTION

Directional solidification is both a useful means of controlling microstructures of materials in basic investigations and a potentially important industrial process for manufacture of in-situ composites. Applications of directional solidification techniques to eutectic alloys have been concentrated mainly in the class of eutectic alloys in which both phases have low entropies of fusion such as Pb-Sn, Sn-Cd, Sn-Zn and Al-Zn (1) resulting in lamellar or rod-like morphologies.

A second class of eutectic alloys is that in which only one phase has a low entropy of fusion (e.g. Pb-Bi, Sn-Bi). Among these alloys is the Al-Si eutectic which has a long history as the basis for industrial casting alloys (2). The phase diagram of the Al-Si system is shown in Fig. 1. As is characteristic of alloys in this class, when the alloy is rich in the low entropy phase (Al), the high entropy phase (Si) solidifies as primary crystals (1).

The purpose of this work has been to determine the effect of directional solidification on the yield strength of Al-Si eutectic and relate the yield strengths to the various microstructures present.

II. BACKGROUND

Suppression of independent growth of primary Si crystals is one of the prerequisites of a well-aligned in-situ composite. The following relationship (3) defines the conditions needed:

$$G/R \geq \frac{mC_s(1 - K_o)}{DK_o}$$

where: m = liquidus temperature gradient

$K_o = C_s/C_l$ = distribution coefficient

C_s = composition of solid phase

C_l = composition of liquid phase

D = diffusion coefficient in liquid ahead of solid/liquid interface

Published information (3) on the effect of variations in growth rate and temperature gradient on this metal-non-metal eutectic identified three important regions (Fig. 2).

Region A: The very high G/R ratio in this region produces large, interconnected, faceted Si crystals with a high incidence of {111} growth twins. These crystals project into the liquid ahead of the essentially planar and isothermal Al growth front (3).

Region B: In this region the silicon crystals assumed a variety of shapes and shared a nearly perfect [100] fiber texture. As has been reported in other directional solidification experiments (4), the preferred texture did not develop for the first few centimeters of the ingot.

The Si crystals grew in the form of high aspect ratio rods with side plates branching out radially. These side plates have been compared (3) to the secondary branches of dendrites, and were of two forms (Fig. 3); thin smooth {100} plates, or corrugated {111} plates with alternate sheets having (111) and ($\bar{1}$11) orientations. Throughout this region there were areas where large silicon crystals were joined together in "instability bands" (3), rich in silicon and lying normal to the growth direction. The Si rich bands were interspersed with Al rich bands which

have Si contents much lower than that of the eutectic composition.

Region C: With an increase in R to greater than ca. 1.0 cm/h the characteristic texture of Region B is no longer found; Si crystals are smaller in size and spaced closer together. An increase in the density of {111} Si growth twins was reported by Day and Hellawell (3) in this region. The microstructures characteristic of this region corresponded more closely to those found for typical cast alloys.

The aluminum phase in Regions A, B, and C shows no orientation relationship to the growth direction or to the silicon phase.

Previous Work: The previous investigation of the tensile properties of directionally solidified Al-Si eutectic, by Steen and Hellawell (5), was concerned only with Region C (growth rates from 3.6 cm/h to 2880 cm/h through temperature gradients from 110^{o} c/cm to 230^{o} c/cm) using thin (4.5 mm dia) long (25 mm) solidification ingots. These authors concluded that cracks propagated along the faces of Si "flakes". There was no attempt at yield strength measurements at various growth rates.

This author's work measured tensile properties of alloys solidified at both the higher growth rates previously studied, and also at growth rates below the transition point between the morphologies found in Region B and Region C. The intention of these tensile measurements was to relate trends in the tensile strength of the alloy to the microstructure effects resulting from directional solidification.

III. EXPERIMENTAL

Master ingots of the eutectic composition were prepared from 99.999 percent purity aluminum and silicon. Solidification boats were fabricated

from Norton #24163 (Alumdum) combustion boats by cutting one end to fit into a carbon chilling block (Fig. 4). Directional solidification was accomplished through the use of a quartz tube (diameter 4.6 cm) which passes through the center of a movable, horizontal furnace (Fig. 5).

The solidification process starts with the combustion boat containing approximately 100 grams of the master ingot placed within the quartz tube; which is evacuated and filled with argon gas to approximately two atmospheres. The furnace is then positioned around the boat and the sample ingot is heated in a molten state (ca. 1000^{o}C) for eight hours. Next a drive mechanism withdraws the furnace at the prescribed growth rate, R, which is taken to be the freezing rate. A copper cooling flange designed for the mouth of the furnace helps supply the temperature gradient necessary for solidification. Data of temperature versus furnace position was obtained using a chromel-alumel thermocouple glued into a slot machined in the bottom of the solidification boat. From this temperature profile the temperature gradient G at the liquid solid interface was determined. Directionally solidified ingots were obtained for a series of growth rates ranging from 0.097 cm/h to 47 cm/h through a temperature gradient of approximately 80^{o}C/cm (Fig. 2). Cast microstructures were obtained using a water quench. The frozen ingots were characteristically 20 cm long with an average cross section of 1 cm by 2 cm. Because there are disturbed regions at the ends of directionally solidified ingots (4), only the center section was used for both metallographic and tensile specimens. Prior to metallographic examination, transverse and longitudinal sections were polished and etched with Kellers reagent.

Flat tensile test specimens were fabricated from the directionally solidified ingots as specified by ASTM-E8-69 (Standard Methods of Tension Testing of Metallic Materials). The long axis of the tensile specimen was parallel to the growth direction (longitudinal direction). Rectangular (subsize) specimens were used with a final thickness of approximately 0.165 cm (gage length, 25mm; width, 6.25mm). These specimens were tested on an Instron two screw tensile machine, using a constant cross-head rate of 0.1 cm/hr. A non-averaging extensometer was attached to each specimen to record the strain versus load. The yield strength values were then found using a 0.2% off-set method as described in ASTM-E8-69.

After tensile testing, the fracture faces were examined using a JOEL JSM-U3 Scanning Electron microscope. X-ray Transmission Laue photographs were taken of specimens thinned to approximately 0.031 cm using Ni filtered CuK radiation at 40 KV, and 20 ma. Specimen to photographic plate distance was 4 cm and the exposure time averaged 60 minutes.

IV. RESULTS

Microstructures: Typical microstructures obtained in this work are shown in Figs. 6a-6h. There are two significant features of these photomicrographs. At growth rates greater than about 1 cm/hr (the higher growth rate regime) both the longitudinal (6a and 6c) and the transverse (6b and 6d) micrographs show a similar arrangement of high-aspect ratio Si crystals (the dark phase) randomly arranged within the matrix. At growth rates less than 1 cm/hr (the lower growth rate regime) the microstructure present showed a marked difference between the transverse (Figs. 6f and 6h) and longitudinal (Figs. 6e and 6g) micrographs. These

latter photomicrographs suggest a composite-like structure composed of Si "rods" (with radial plates), aligned parallel to the growth direction within a matrix of aluminum.

Examples of a second type of microstructure found in the lower growth rate region are illustrated in Fig. 7. The dark, Si-rich bands, composed of massive Si crystals, are prominent at both of the growth rates shown. These bands are of irregular length; and there is a decrease in the spacing between bands with an increase in the growth rate from 0.097 cm/h to 0.25 cm/h. Comparison between Fig. 7a and 7d (both at the same magnification) clearly shows this decrease in spacing with growth rate, though the limited number of growth rates sampled restricts a more quantative analysis. At the growth rate of 0.25 cm/h the Si depleted bands (white bands) are quite regular and extend across the entire width of the specimen.

X-ray Investigation: Typical Transmission Laue photographs are shown in Fig. 8. In the higher growth rate region there are concentric spotty Debye rings for both the Si and Al phases (Figs. 8a and 8b). The Debye rings from the Si phase concentrate into arcs in the lower growth rate region, but the rings for the Al do not (Figs. 8c and 8d). The transition to the arc pattern is at the same growth region as that of the aligned silicon microstructure.

Tensile Tests: Sample stress-strain curves obtained for the higher growth rate regime are shown in Fig. 9. The yield strength as well as the strain to failure follow a general trend with R. Due to experimental difficulties with recording portions of the strain data during tensile

testing; a complete set of elastic modulus data could not be determined. Yield strength values derived from data such as from Fig. 9 are shown in Fig. 10. For reasons discussed later, an abscissa of $R^{1/4}$ was chosen. There are two general regimes evident in these data which coincide roughly with those found previously in the photomicrographs. Below R ca. 1.0 cm/hr the yield strength appears to be independent of growth rate. However, for higher growth rates the yield strength curve is linear up to the highest rate used. The range of yield strengths in this regime fell between that of a chill cast specimen and the matrix component; essentially Al 1100.

SEM: Qualitative features of the fracture modes were investigated using a scanning electron microscope, Fig. 11. In the higher growth rate regime, Figs. 11a and 11b, the arrangement of the Si crystals resulted in a random combination of fracture faces at varying angles. There is also some evidence of plastic flow in the aluminum. At the lower growth rates, Figs. 11c, 11d, the fracture faces show a high volume fraction of massive Si crystals.

V. DISCUSSION

Microstructure: The photomicrographs shown in Fig. 6 corroborate the basic features of the work of Day and Hellawell (3). However, our investigation was concerned only with one temperature gradient (ca $80^{\circ}C$/cm), so no comparison with Region A in Fig. 2 could be made. The effect of changes in the growth rate on the morphology and spacing of the silicon crystals is evident in the photomicrographs. Those taken of samples in Region B verify the reported fiber texture and show the zig-zag pattern

which results when one of the {111} side plates is cut parallel to the fiber axis (Figs. 6e and 6g). The most striking change in morphology is the loss of texture when the growth rate changes from 4.6 cm/hr and 0.01 cm/h. Both the size and dispersion of the Si crystals is seen to qualitatively decrease as the R increases in both the lower and higher growth rate regions.

Banded Microstructures: The "instability bands" reported by Day and Hellawell were quite prominent in the lower growth rate region. Whereas these authors characterized the instability bands as "interconnected, fiberous crystals"; as shown in Fig. 7, the bands found by this worker were made up of aggregates of large silicon particles. The Si-rich bands had a width of the order of 500μ, being composed of Si crystals varying in size from 50μ-100μ in diameter (Figs. 7b and 7c). The Si depleted bands were narrower (ca 20-50μ) and were made up of a much finer dispersion of Si particles (Figs. 7c and 7d). Electron beam microprobe investigations showed the volume fraction of Si in the Si-rich bands to be about 0.5, dropping to less than about 0.02 in the Si depleted bands.

As mentioned earlier, there is a qualitative decrease in the distance between the Si rich bands with an increase in R from 0.097 cm/h to 0.25 cm/h, though the irregular nature of the bands and the limited data from two growth rates limits quantitative comparison to R. The banded microstructure was found only in the central portions of the directionally solidified ingots. Comparison between Fig. 7 and the lower growth rates of Fig. 6 indicate the texture evident in Figs. 6e and 6g is not found within the areas of banded microstructure.

The factors governing the transition from the aligned microstructure to the banded microstructure are not totally understood at this point in our work. The alloys characterized by Day and Hellawell (3) were directionally solidified at growth rates and temperature gradients similar to those used in this work, but the solidification apparatus was different. The vertical solidification apparatus and smaller diameter of the ingots grown by these workers may partially explain the difference between the bands found in their work and this work.

Texture: Verification of the reported (2, 4) [100] fiber texture of the {111} side plates characteristic of portions of Region B is supplied by transmission laue photographs shown in Fig. 8. This {100} fiber texture is illustrated in a stereographic projection shown in Fig. 12. Comparison between Figs. 10c and 10d with the stereographic projection verifies the relationship between the {100} and the twinned {111} side plates and the growth direction. The polycrystalline nature of the aluminum results in the characteristic Debye rings regardless of the growth rate, while the silicon rings disappear at the transition between Regions B and C. The radial lines in the photographs are the result of the short wavelength radiation still present in the filtered CuKα x-ray beam.

The Effect of the Growth Rate on Inter-rod Spacing: Measurements on the photomicrographs were used to estimate a mean inter-fiber spacing, λ, in Region C. The method used was to take linear traverses of a transverse section, count the number of intersections (with silicon micro-crystals), divide by twice the width of the transverse section and multiply by the volume fraction of the Al phase. This procedure was repeated at least

ten times on parallel lines and then an average was taken. A summary of the results is presented in Fig. 13. Data obtained by Hellawell (3) for irregular microstructures in the Al-Si system are also plotted in Fig. 13. Only a qualitative comparison can be made, since their data for a different temperature gradient (G = 30^{o} C/cm). However, the data strongly suggest $\lambda^2 R$ = constant in both instances.

The Effect of the Growth Rate on the Yield Strength

Higher Growth Rate Region: As first observed by Pacz (2), the cast eutectic Al-Si alloy fractures along the sharp faces of the randomly arranged Si crystals. As discussed earlier, the effect of growth rate on the spacing between Si crystals (Fig. 13) suggests the following relationship:

$$\lambda^2 R = \text{Constant} \qquad (1)$$

Initial analysis of the yield strength values for specimens in this growth-rate region suggested a strong relationship between the Si crystal spacing and the yield strength values. Various graphical representations were attempted to determine the dependence of yield strength on growth rate, resulting in Figure 9. A linear relationship between $R^{1/4}$ and yield strength is evident in the higher growth region of figure 9. This relationship can be represented as follows:

$$\sigma = \text{constant} + CR^{1/4} \qquad (2)$$

Combining equations (1) and (2) results in a relationship between the yield strength and the inter-crystal particle spacing:

$$\sigma = \text{constant} + C'\lambda^{-1/2} \qquad (3)$$

Further analysis of the nature of the yielding in the higher growth-rate region is supplied by comparing Equation 3 to the much studied Hall-Petch relationship; relating the yield stress to grain size:

$$\sigma = \sigma^* + KL^{-1/2} \tag{4}$$

where

σ = Yield or Rupture Stress

σ^* = Internal Stress

K = Hall-Petch Slope

L = Grain Size of Interfiber Spacing, λ.

Although the mechanisms governing this relationship are not clear (4), the application of Equation 4 to two phase materials has been found valid when the difference in the modulus of elasticity of the two phases is great (9, 10) and when there is a good bond at the interface between the two phases (11).

Since the modulus of elasticity of Si is approximately three times that of Al, The high aspect ratio Si crystals act as a strong reinforcing phase. As seen in Fig. 9, there is considerable yielding at an almost constant stress before fracture, showing the strengthening effect of the randomly spaced Si particles. In the scanning micrographs (Fig. 11) of the fracture faces, it can be clearly seen that the fracture was predominantly along Si cleavage faces.

Li and Chou (10) have discussed at length the flow stress-grain size relationship. The Hall-Petch relationship is obtained for a variety of models. They point-out that "Yielding is to take place when stress concentration reaches the strength of the grain boundary." In our work

there are two separate phases. The applicability of the Hall-Petch relationship in this case is also discussed by Li and Chou (10). Here yielding in aluminum starts before the stress reaches the fracture stress of the Si phase. Thus, although the fracture takes place in the silicon phase, the Hall-Petch relationship is applicable to the yielding in aluminum.

Lower Growth Rate Region: An initial impetus for this work was the possible effects of the aligned Si structures in the lower growth rate region on the yield strength. But, with the combination of the large Si crystals surrounded by a matrix of almost pure Al, the yielding is dominated by the stress concentrations arising within the Si-rich bands. The irregularly shaped Si crystals prematurely cleave resulting in a yield strength approaching that of pure aluminum. The nature of the yielding in this region does not allow a quantitative analysis of the strength of the aligned growth region.

In several metal-metal and non-metal-non-metal systems (17) directional solidification has produced composites (aligned microstructures). A stress analysis of the aligned microstructures would consider the high-aspect Si crystals as reinforcing rods in a matrix of Al. The simplest model of this composite assumes that the bond between the two phases is capable of transferring stresses which develop due to the differing elasticities of the two phases.

For stresses within the elastic regime, the simple rule of mixtures describes the composite stress as a function of the volume fraction:

$$\sigma_C = \sigma_R V_F + \sigma_M V_M$$

where,

σ_C = Stress in Composite

σ_F = Stress in Rod

σ_M = Stress in Matrix

V = Volume Fraction

This relationship can be modified to take into account the orientation of the re-enforcing phase (8), the variability in length of the re-enforcing phase (16), and the strain hardening within the matrix.

The strengths of casting alloys similar to the alloy tested are dependent upon the re-enforcing offered by the silicon crystals (modified) dispersed in the Al matrix. Alignment of the Si phase would increase the strength due to the cooperative effect of the two phases on the stress distribution. This added strength would, of course, only be in a direction parallel to the direction of alignment of the Si "rods". The Al phase, acting as the composite matrix, would distribute loads between the Si "rods" by a shear mechanism.

The benefit of this metal-matrix composite structure is not only the added strength, but also the quality of the bond between the two phases. The major failing of most fabricated composite materials is their inability to efficiently transfer loads between the matrix and strengthening phases. The interphase bond in directionally solidified alloys is characteristic of high integrity, improving both fatigue and high temperature characteristics.

V. CONCLUSION:

Directional solidification of the eutectic Al-Si alloy, over a range of growth rates, was carried out; tensile specimens fabricated, and longitudinal yield strengths measured. The yield strengths for growth rates greater than ca. 1.0 cm/hr were dependent upon the spacings of the Si particles, following a Hall-Petch type relationship. The yield strengths of alloys solidified at rates lower than ca. 1.0 cm/hr were dominated by preferential yielding within Si-rich bands lying normal to the growth direction. Possible composite strengthening due to aligned Si microstructures in this growth regime was not realized due to this preferential yielding.

REFERENCES

1. J. D. Hunt and K. A. Jackson, Met. Trans. AIME, Vol. 236, p. 843 (1966).
2. A. Pacz, U. S. Patent 1,387,900 (1971).
3. M. G. Day and A. H. Hellawell, Proc. Royal Soc., A 305, pp. 473-491 (1971).
4. G. A. Chadwick, Prog. Materials Science, 12, No. 2, 99 (1963).
5. H. A. H. Steen and A. H. Hellawell, Acta. Met., 20, 363 (1972).
6. B. D. Cullity, X-ray Diffraction, Addison-Wesley, Co., (1956).
7. A. S. Yue, Met. Trans. AIME, 224, 1010 (1962).
8. F. D. Lemkey, R. W. Hertzberg and J. A. Ford, Met. Trans. AIME, 233 334 (1965).
9. H. Bibring, Conf. on In-Situ Composites (Proc.), 2, 12-15 (1972).
10. J. C. M. Li and Y. T. Chou, Met. Trans., 1, 1145 (1970).
11. Y. T. Chou, Can. J. of Phys., 45, 559 (1967).
12. B. J. Shaw, Acta Met., 15, 1169 (1967).
13. L. J. Broutman and R. H. Krock, Composite Materials, Vol. 5 Academic Press (1974).
14. W. D. Sylwestrowicz, Phil. Mag. 7, 1825 (1962).
15. K. R. Van Horn, Aluminum, ASM, 1967.
16. F. W. Crossman, A. S. Yue, and A. E. Vidoz, Met. Trans. AIME, Vol. 245, pp. 397-406, (1969).

FIGURE CAPTIONS

Fig. 1. Phase diagram of aluminum-silicon, Ref. 15.

Fig. 2. Temperature gradient (G) and growth rate (R) of test alloys.

Fig. 3. Idealized drawing of Si crystal, in lower growth region, showing crystallography of side plates and growth direction, Ref. 3.

Fig. 4. Carbon chilling block and solidification boat.

Fig. 5. Directional solidification apparatus.

Fig. 6a. Photomicrography of longitudinal section (R = 0.1 cm/hr) (magnification 100x).

Fig. 6b. Photomicrograph of transverse section (R = 0.1 cm/hr) (magnification 100x).

Fig. 6c. Photomicrograph of longitudinal section (R = 0.97 cm/hr) (magnification 100x).

Fig. 6d. Photomicrograph of transverse section (R = 0.97 cm/hr) (magnification 100x).

Fig. 6e. Photomicrograph of longitudinal section (R = 4.6 cm/hr) (magnification 100x).

Fig. 6f. Photomicrograph of transverse section (R = 4.6 cm/hr) (magnification 100x).

Fig. 6g. Photomicrograph of longitudinal section (R = 23.0 cm/hr) (magnification 100x).

Fig. 6h. Photomicrograph of transverse section (R = 23.0 cm/hr) (magnification 100x).

Fig. 7a. Photomicrograph of instability bands lying normal to growth direction (R = 0.1 cm/hr).

Fig. 7b. Photomicrograph showing large Si crystals within instability

bands (R = 0.1 cm/hr).

Fig. 7c. Photomicrograph of instability bands in low growth rate region (R = 0.25 cm/hr).

Fig. 7d. Detail of Fig. 6c showing various types of banding.

Fig. 8a. Transmission Laue Photograph (R = 23.0 cm/hr).

Fig. 8b. Transmission Laue Photograph identifying Debye Rings (R = 2.4 cm/hr).

Fig. 8c. Transmission Laue Photograph (R = 0.25 cm/hr).

Fig. 8d. Transmission Laue Photograph (R = 0.97 cm/hr).

Fig. 9. Stress/strain curves for directionally solidified alloys.

Fig. 10. Variation of yield strength with $R^{1/4}$.

Fig. 11a. SEM photograph (R = 4.6 cm/hr) magnification 300x.

Fig. 11b. SEM photograph (R = 23.0 cm/hr) magnification 300x.

Fig. 11c. SEM photograph (R = 0.1 cm/hr) magnification 300x.

Fig. 11d. SEM photograph (R = 0.097 cm/hr) magnification 300x.

Fig. 12. Stereographic projection of [100] texture of {111} side plates.

Fig. 13. Relationship between inter-lamella spacing and growth rate.

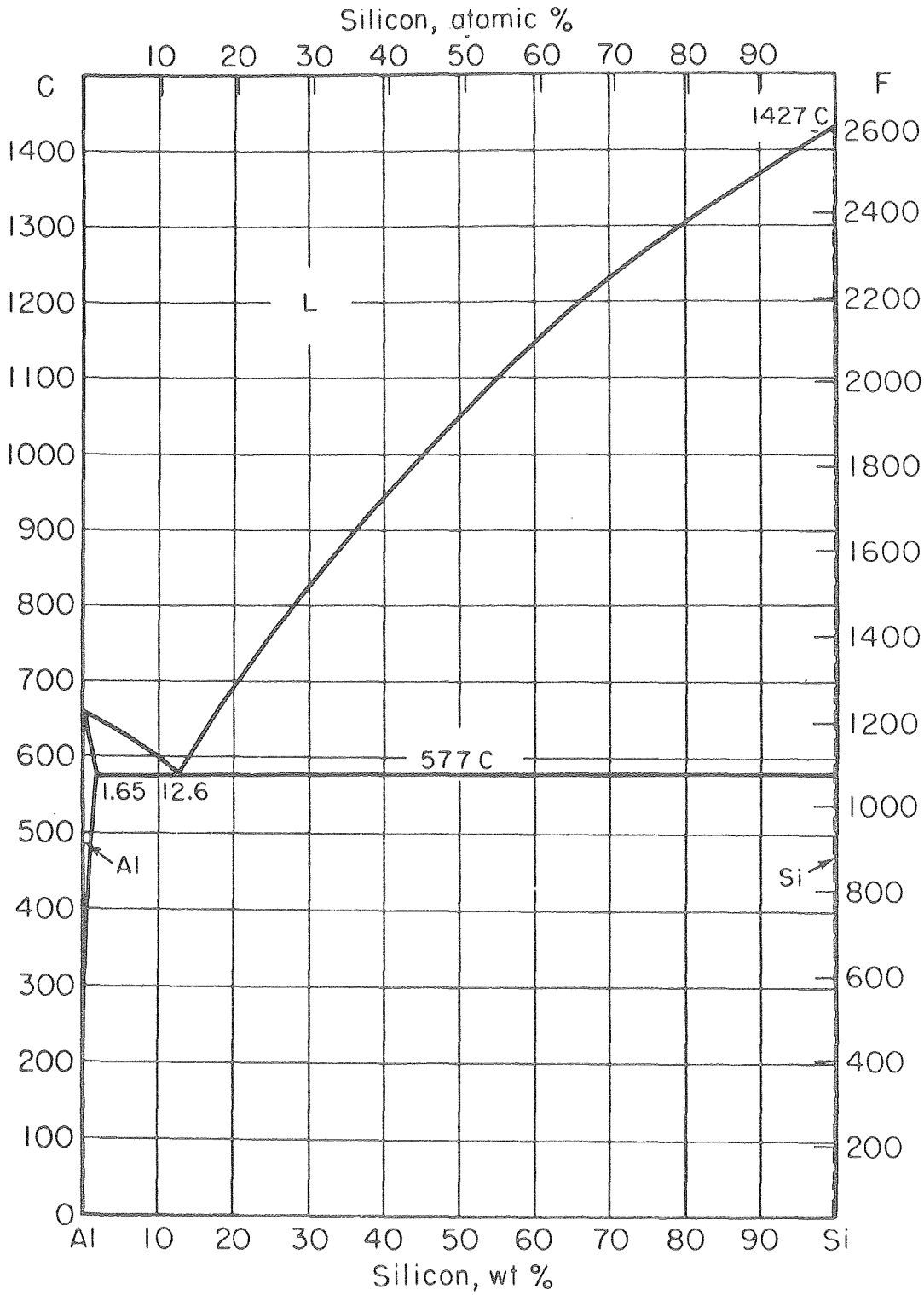

XBL 7512-10076

Fig. 1

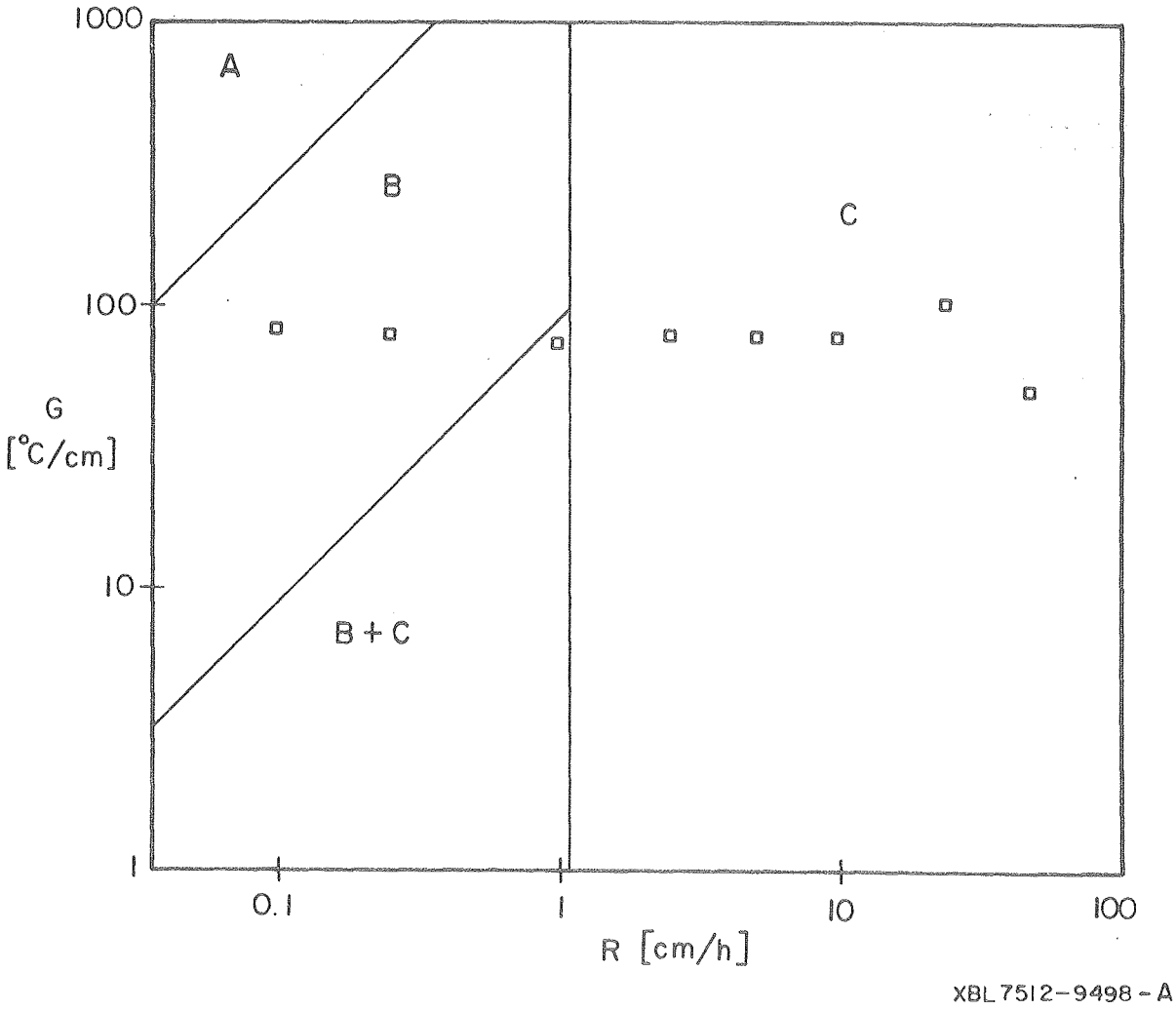

Fig. 2

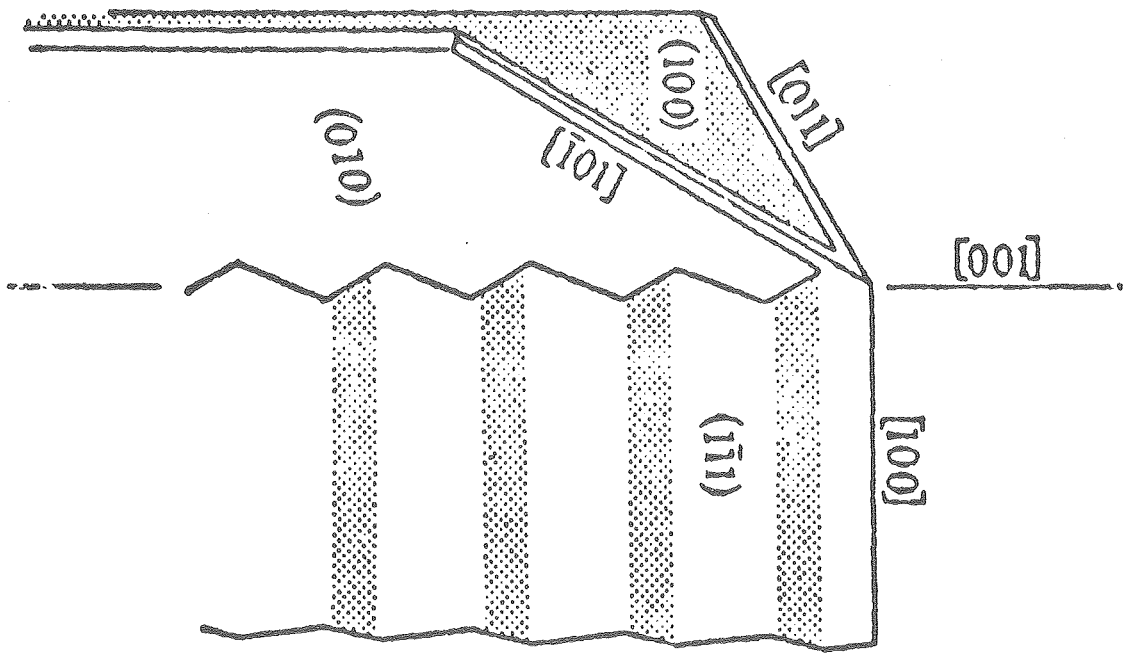

Fig. 3

XBL 763-754

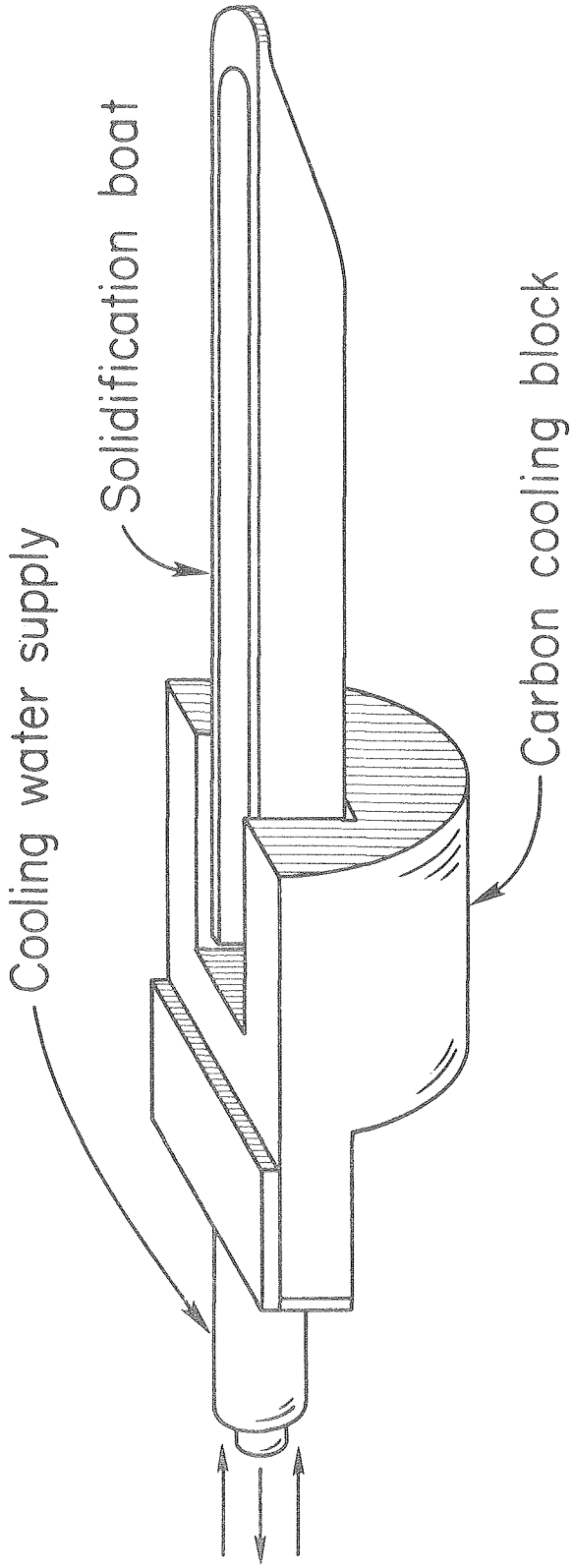

XBL7512-10080 A

Fig. 4

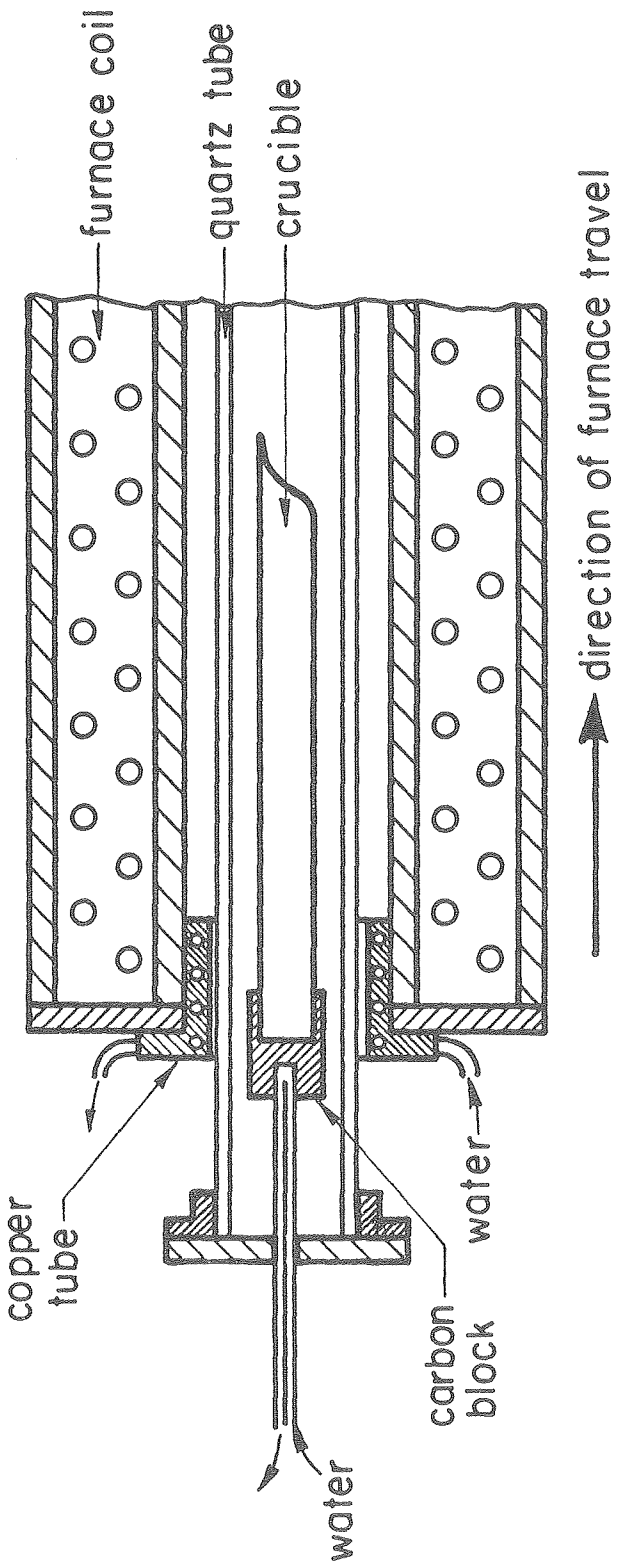

XBL7512-9251

Fig. 5

Fig. 6a (R = 4.6 cm/h)

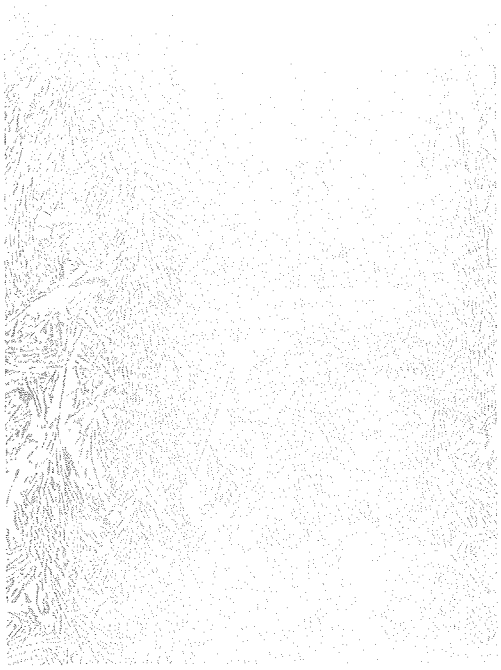

Fig. 6c

Growth Direction

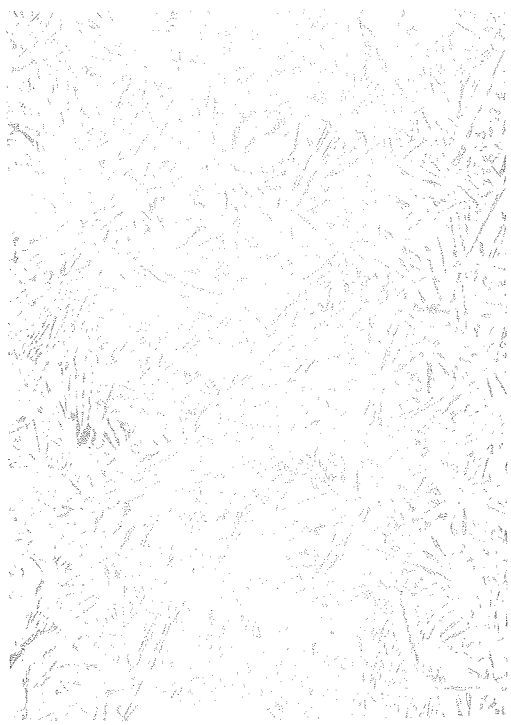

Fig. 6b

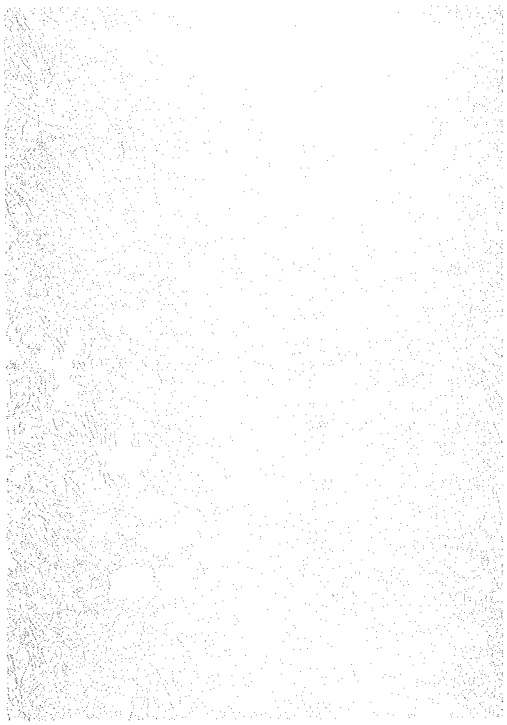

Fig. 6d

XBB 7512-9076

200μ

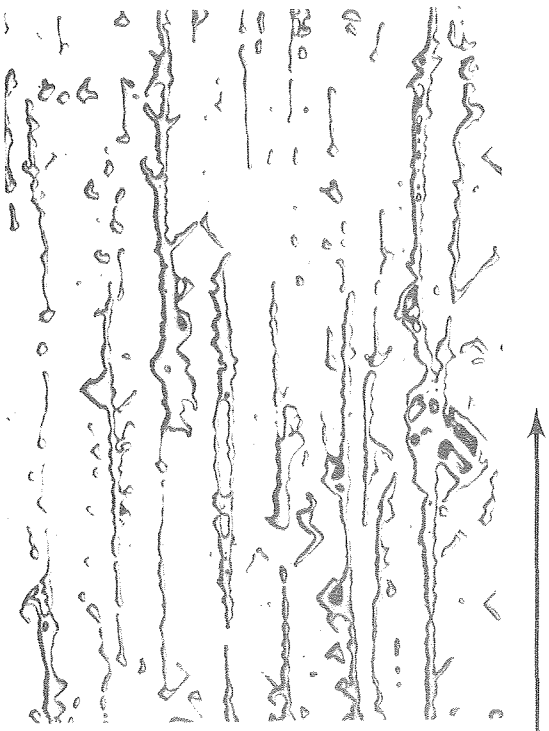

Fig. 6e
(R = 0.097 cm/hr)

Fig. 6g
(R = 0.25 cm/hr)

Growth Direction

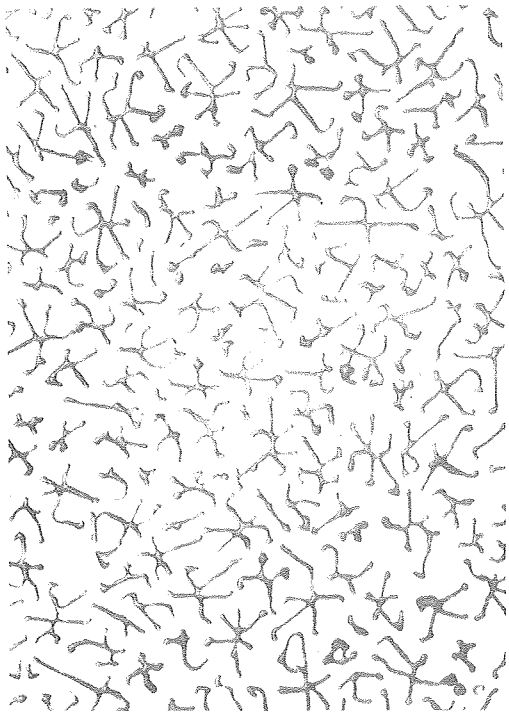

Fig. 6f

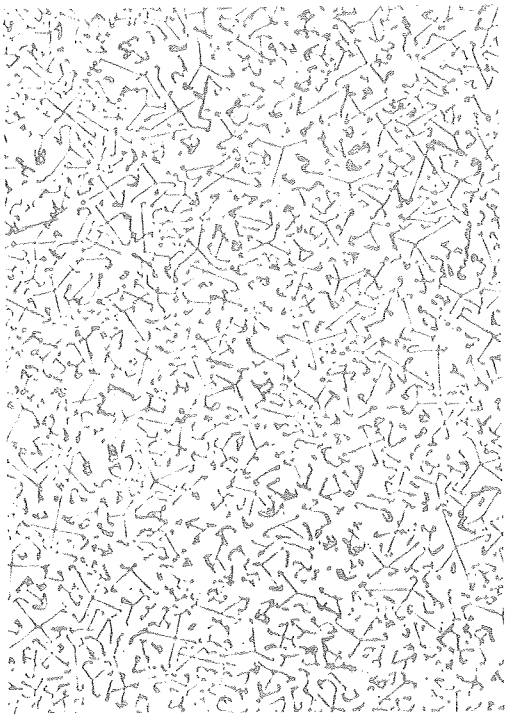

Fig. 6h

XBB 7512-9072

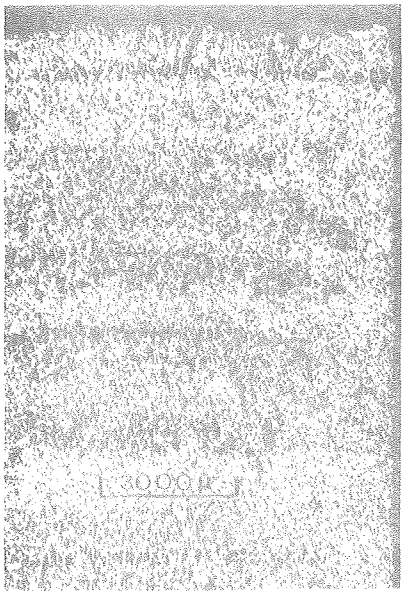

Fig. 7a

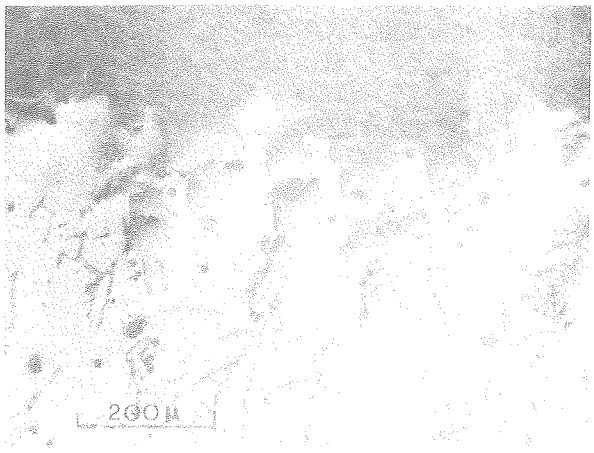

Fig. 7b

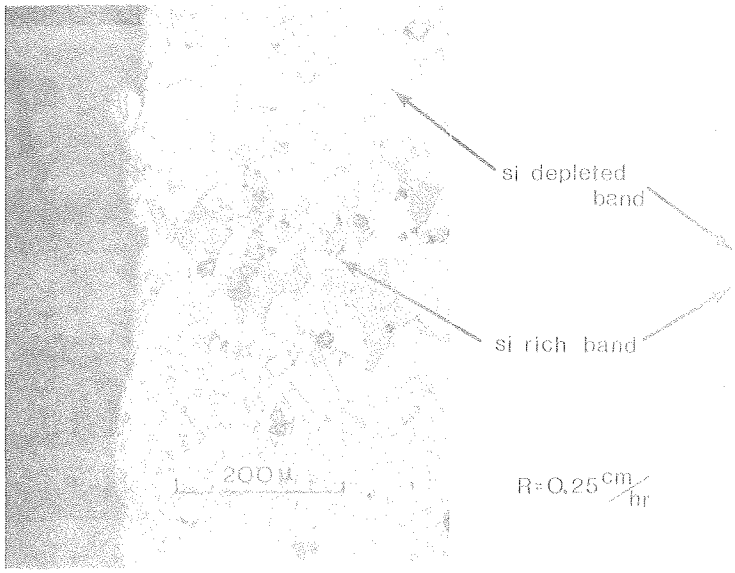

Fig. 7c

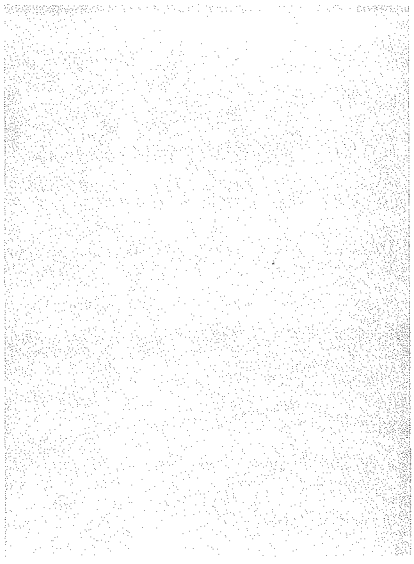

Fig. 7d

XBB 762-1304

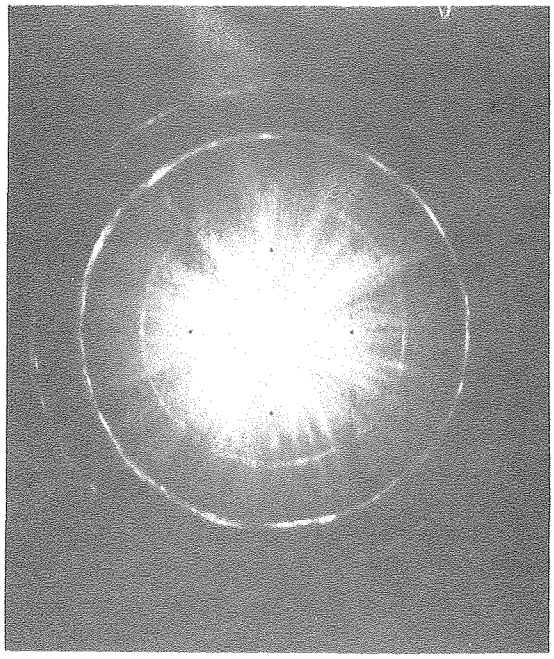

Growth Direction

Fig. 8a R = 23.0 cm/hr

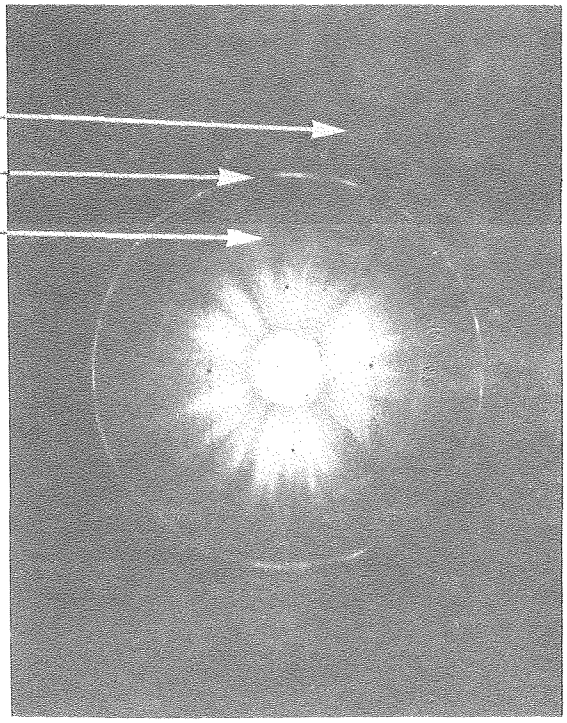

Fig. 8b R = 2.4 cm/hr

XBB 7512-9073

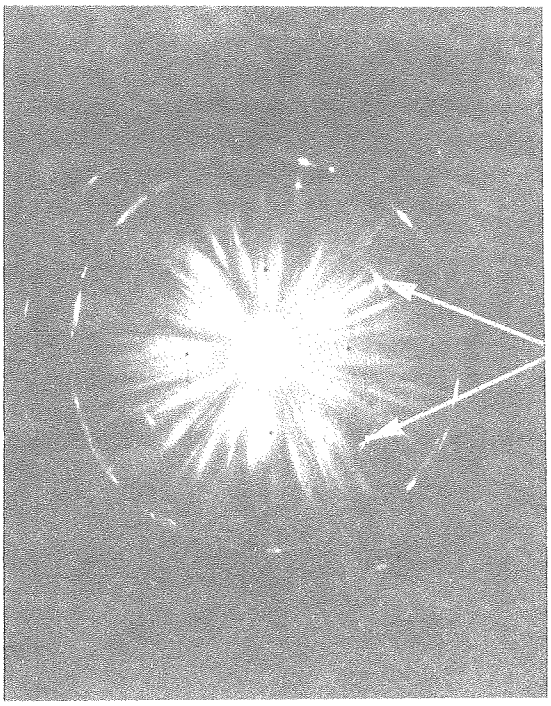

Fig. 8c. R = 0.45 cm/hr
Arcs resulting from [200] fiber texture of [111] Si crystals

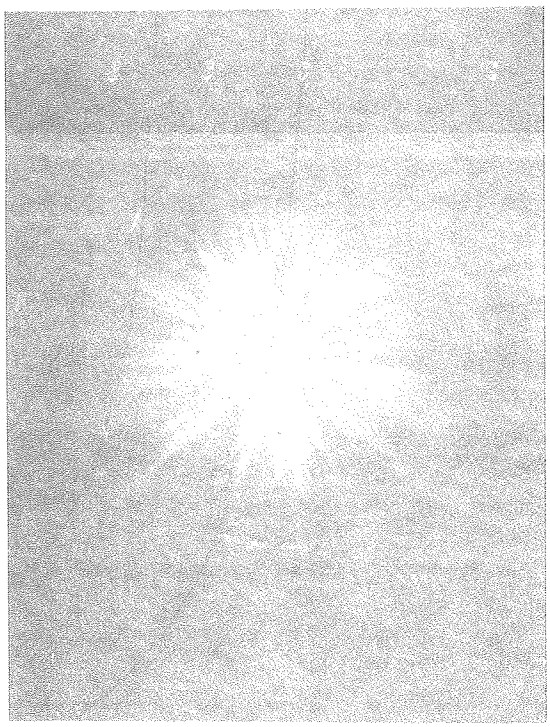

Fig. 8d. R = 0.97 cm/hr

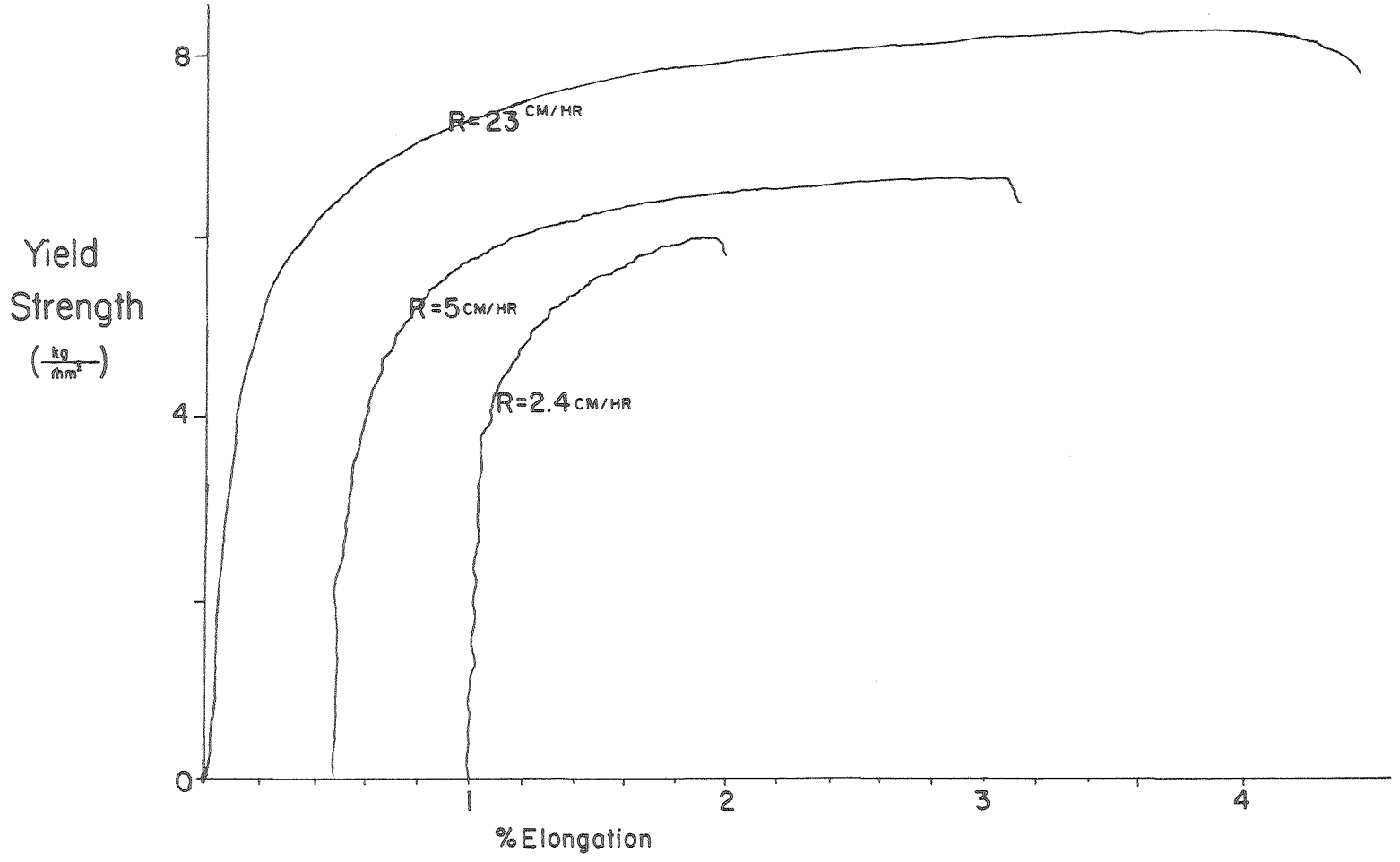

XBL 7512-10081A

Fig. 9 (NOTE: Separate zero points taken for each growth rate.)

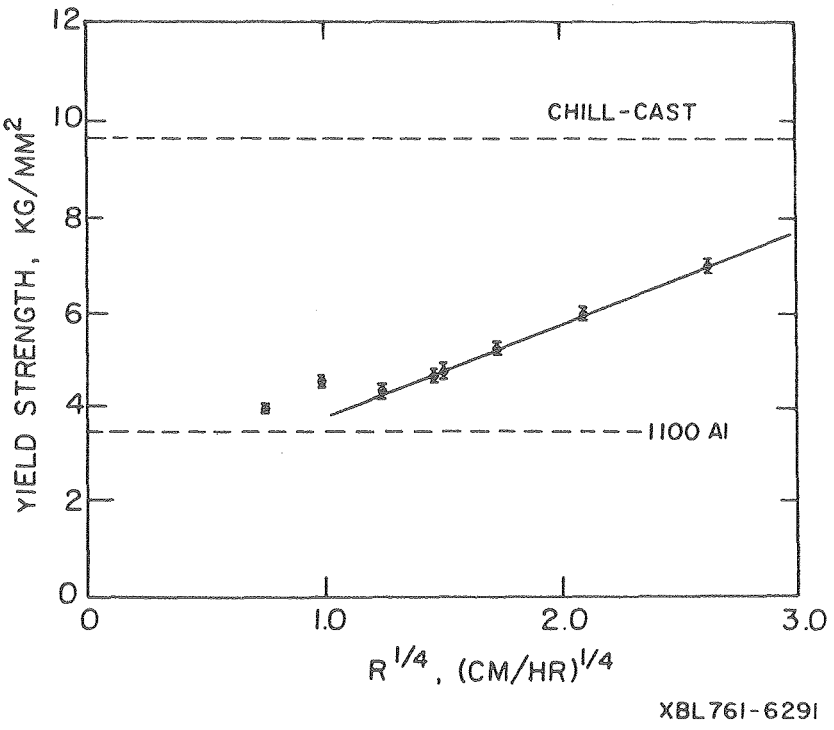
12
10
8
6
4
2
0
YIELD STRENGTH, KG/MM²
CHILL-CAST
1100 Al
0
1.0
2.0
3.0
R 1/4, (CM/HR)1/4
XBL761-6291

Fig. 10

Fig. 11a (R = 4.6 cm/hr)

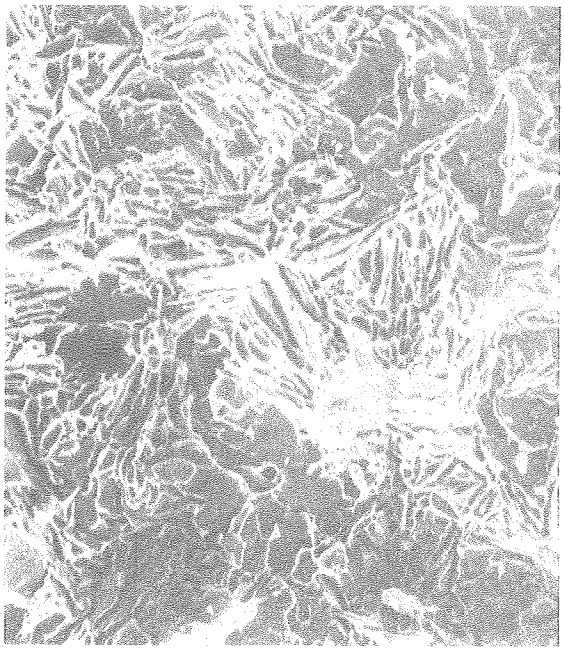

Fig. 11b (R = 23.0 cm/hr)

100 μ

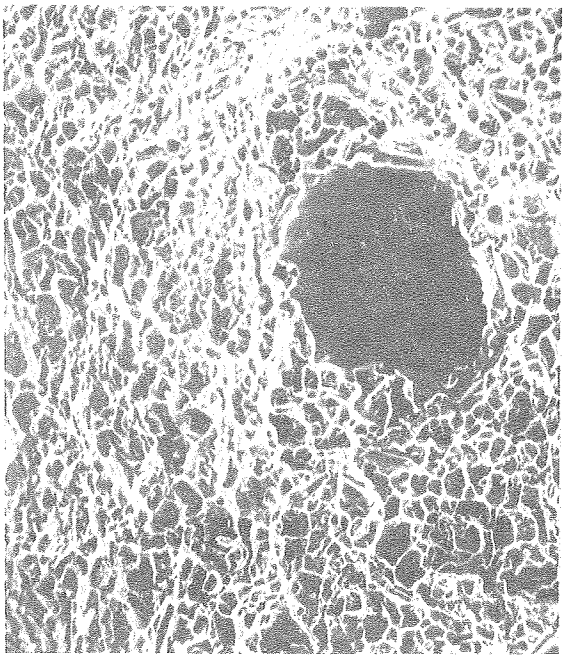

Fig. 11c (R = .97 cm/hr)

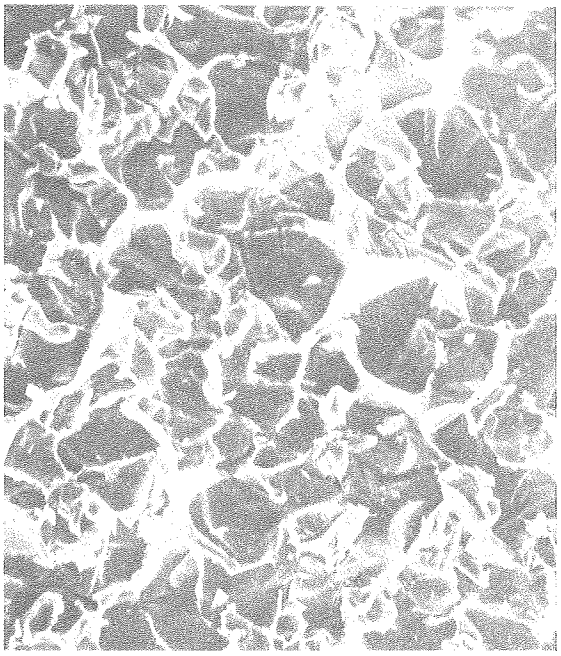

Fig. 11d (R = .097 cm/hr)

XBB 7512-9071

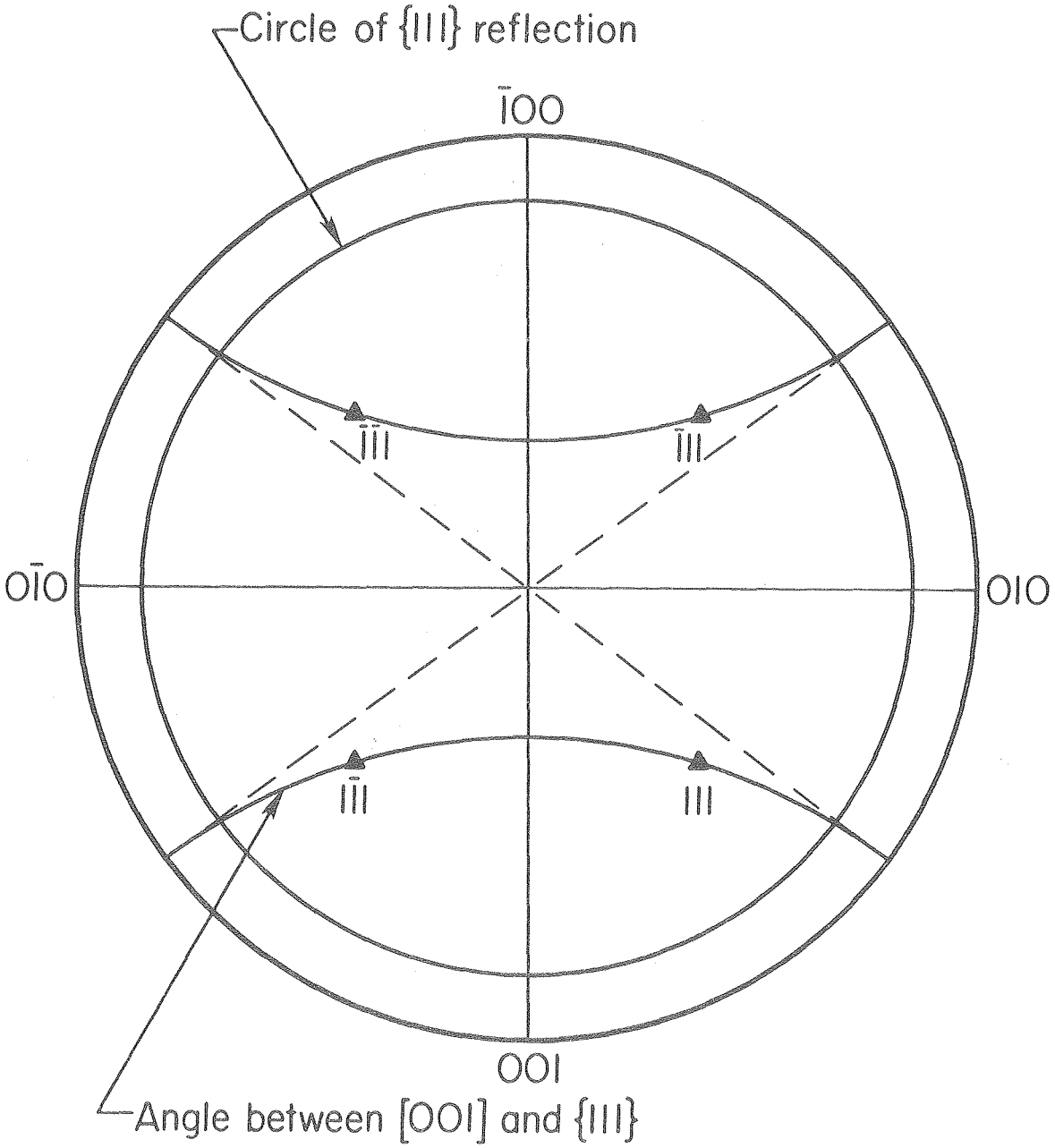

XBL 763-2445A

Fig. 12

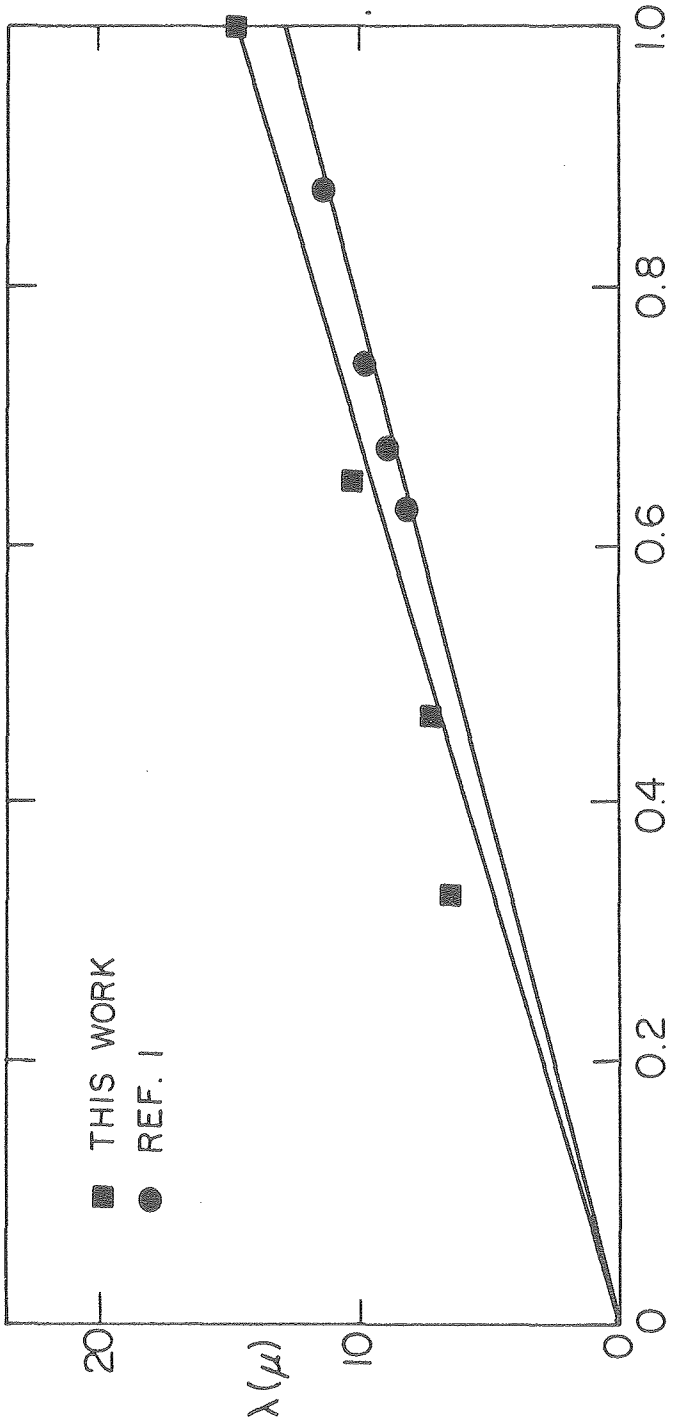

Fig. 13

This report was done with support from the United States Energy Research and Development Administration. Any conclusions or opinions expressed in this report represent solely those of the author(s) and not necessarily those of The Regents of the University of California, the Lawrence Berkeley Laboratory or the United States Energy Research and Development Administration.